Kalman Smoother Based Force Localization and Mapping Using Intravital Video Microscopy

Dejan Lj. Milutinović*
Assistant Professor
Applied Mathematics and Statistics Department
Baskin School of Engineering
University of California
Santa Cruz, California 95064, USA
Email: dejan@soe.ucsc.edu

Devendra P. Garg
Professor, Fellow of ASME
Department of Mechanical Engineering and Materials Science
Duke University
Durham, North Carolina 27707, USA
Email: dpgarg@duke.edu

ABSTRACT

Motility is an important property of immune system cells. It provides cells with the ability to perform their function not only at the right time, but also at the right place. In this paper, we introduce the problem of modeling and estimating an effective force field directing cell movement by the analysis of intravital video microscopy. A computational approach is proposed for solving this problem without dealing with a parameterized spatial model of the field in order to avoid potential errors due to inaccurate spatial model assumptions. We consider the dynamics of cells similar to the dynamics of distributed agents typically used in the field of swarm robotics. The method utilizes a fixed-interval Kalman filter based smoother. Its application results in a map giving the intensity and direction of the effective force field. The results show that real-time video images are a source of data, enabling us to visualize intriguing spatio-temporal phenomena inside immune system organs. The proposed approach can fill the existing gap between contemporary technology and quantitative data analyses present in the field of biosystems. [1]

1 Introduction

The lymph nodes are secondary lymphoid tissues and anatomical sites where, along with the spleen, the major component processes of the immune response to infection and vaccination occur, including antigen recognition, cellular activation,

*Address all correspondence to this author.
[1]This work was supported by the Army Research Office under Short Term Inovative Research (STIR) grant number W911NF-07-R0003 and grant number W911NF-08-1-0106.

differentiation, affinity maturation and the establishment of immune memory. Recent advances in imaging technology provide us a novel insight into the dynamics of immune cell interactions in intact lymph nodes [1–3].

In this paper, we introduce the problem of estimating the effective force field influencing cell motility based on intravital video microscopy. We name this problem *force localization and mapping*, or FLAM. Considering an individual cell as an agent [4], we find this problem similar to a well-studied problem in robotics, the so-called *simultaneous localization and mapping*, or SLAM [5,6]. In both problems, the estimation is based on the individual agent's motility model and the outcome is a map that visualizes the spatial structure within the agent's environment.

In the immunological context, effective forces originate from the mechanical forces of extracellular environment and the active responses of cells to gradients of chemotactic and haptotactic substances. *Currently, there is no alternative microscopy method available for measuring these forces under physiological condition*. Therefore, we can only rely on a computational method for the effective force field estimation from intravital video microscopy. The estimation provides quantitative information that is important for understanding the behavior of the immune system as a whole. Cellular aggregation and lymphoid tissue morphology are determined largely by these fields and are of great consequence in the development of an effective immune response.

Our emphasis in solving the FLAM problem is the development of an approach that is independent of any assumption about the force field shape. In this way, we hope to avoid an error in the field estimation resulting from possibly wrong intuition; trying, for example, to match the shape of the field to visual patterns in video sequence. By proposing this approach, however, we do not exclude the possibility that after multiple field estimations, as in the case of repeated experiments, the visual patterns can be considered. This will likely prove fruitful once confidence in the relation between the force field shape and the visual patterns has been established.

The data and model that we use in our estimation approach are described in Sections 2 and 3, respectively. Section 4 explains the effective force estimation based on the fixed-interval optimal smoother. We discuss the limitations of this approach in Section 5. Section 6 describes the force estimation in the case of a time-stationary uniform field. The estimation of a non-uniform time-stationary field is introduced in Section 7. Finally, Section 8 presents the conclusions based on this research.

2 Cell motility data

In the case of the lymph-node, cells are $50-250\mu m$ deep in the tissue. The cell motility is observed by two-photon microscopy, which minimizes the damage to cells and surrounding tissue. Two-photon microscopy requires that the observed cells be labeled with fluorescent dyes emitting the light of a specific wavelength when excited by a laser beam. In the case of the experimental setup for lymph-node imaging that we consider, the laser beam typically sweeps out a two-dimensional region of $200 \times 150\mu m$ while its depth in the tissue is varied, providing an image stack of $50\mu m$ thick 3D volume within the lymph-node. We refer to this volume as the *visual field*.

Figure 1 shows a typical 2D image projection of the intra-lymph node image stack in which T-cells and dendritic cells are labeled with two different colors [4]. The sampling interval between subsequent scans of the visual field is in the range

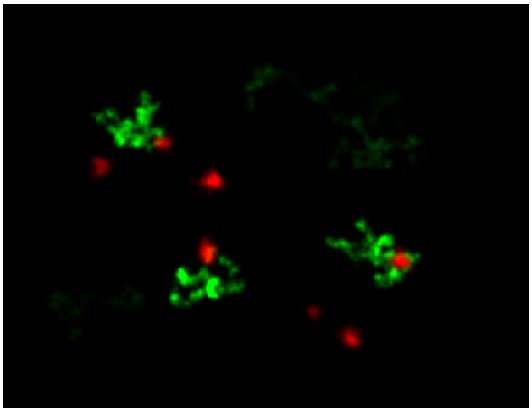

Fig. 1. Computer-generated image of a cellular interaction inside the lymph node: T-cells (red) scan dendritic cells (green) [4]

from 18 to 21 seconds. The data we derive from the stacks are the cell position samples. If each individual cell, i.e., its trajectory, is uniquely labeled by the integer number i, the data we are dealing with are coordinates of cell center x_k^i, y_k^i, z_k^i corresponding to the time points t_k^i along ith trajectory.

Measurement of cell positions from these video images is not error free. To minimize errors, it is necessary to process 3D image stacks, to compensate for distortion introduced by the optical system and transmission of the light through the tissue, prior to measuring the cell positions. Errors in the cell position measurement are mainly to be attributed to finite image resolution and the significant and random change in cell morphology. Moreover, each cell must be assigned to a single trajectory, a task that may be non-trivial when two cell trajectories are in close proximity.

An example of 2D projection of trajectories is depicted in Fig. 2 in which each trajectory is translated back to the origin (0,0). This type of diagram has been previously used [1] to detect the presence of the force. It is obvious that, while we can use the help of such a diagram to detect a constant force, it is not useful if the force field is non-uniform over the visual field. For example, in the case of data presented in Fig. 2, we can see that the force component along the x axis is non-zero and may be constant, but it is difficult to say anything about y-dependence of the force field based on a figure of this type. The cell trajectories presented in Fig. 2 are generated from a realisitic model of cell motility and geometry of the visual field.

We focus on the analysis of data from B- and T-lymphocytes, which have more or less rounded shapes. However, the same analysis can be also applied to motility of irregularly shaped cells, such as macrophages, neutrophils and dendritic cells. It is only necessary that the time-space scale of interest allows that the cell trajectories are fairly well descibed by the cell center positions. Uncertainty of the center position due to the cell shape irregularity can be assigned to the intensity of measurement errors.

3 Cell motility model

According to our general model presented in Fig. 3*a*, an individual cell senses the environment using its receptors and processes received signals intracellularly. Intracellularly generated forces that act on the cell structure arise as a result of this processing. These forces along with mechanical forces act on the cell structure finally resulting in cell movement. While there are attempts to understand chemotaxis in more detail [7–9], in order to estimate effective forces influencing cell motility, we

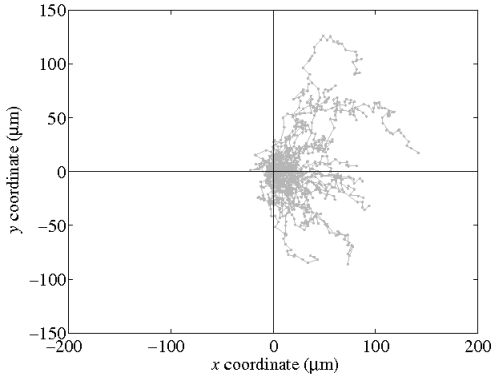

Fig. 2. Two dimensional projection of 40 cell tracks from the 200x150x50 μm visual field provided by two-photon video microscopy (model generated). Each track is translated so that the track begins at the diagram origin. The cells can move in all directions, therefore, the limits for plotting translated trajectories are $\pm 200\mu m$ and $\pm 150\mu m$ along x and y axis, respectively.

use a general model without going into details of intracellular signaling and cell structural properties. This double integrator model representing particle dynamics [10–12] is common in representing the motion of agents in a multi-agent systems.

The model describes motility of an individual ith cell (agent) volume center. The integrator block of the model (see Fig. 3a) diagram does not describe the property of the cell, but the natural relation between cell velocity $\mathbf{v}^i$ and its position $\mathbf{x}^i$. The same relation is presented by the Laplace domain transfer function $\frac{1}{s}$ of the model in Fig. 3b.

Neither the velocity $\mathbf{v}^i$, nor the cell position $\mathbf{x}^i$ can be measured directly. The data we measure directly are cell positions $\mathbf{y}^i$ corrupted by measurement errors θ^i. The error sources are due to limited image resolution, light diffusion and other unpredictable disturbances influencing the detection of the cell volume center. In the model, we assume that the measurement errors $\theta^i(t)$ are additive (see Fig. 3), i.e.,

$$\mathbf{y}^i(t) = \mathbf{x}^i(t) + \theta^i(t) \tag{1}$$

In this notation, vectors $\mathbf{x}^i, \mathbf{v}^i \in R^D$, where $D = 3$ is the spatial dimension. The last equation is called the *observation model* and the additive influence of errors $\theta(t)$ is depicted by the summation symbol Σ in Fig. 3a, as well as in the model in Fig. 3b. We assume that the error distribution is Gaussian zero mean, $\theta^i(t) \sim N(0,\Theta)$, and covariance Θ.

In general, the cell motility velocity is a result of mechanical forces of extracellular environment and the active responses of cells to gradients of chemotactic and haptotactic substances, i.e., extracellular signals (see Fig. 3a). In the model we deal with in this paper (Fig. 3b), persistent component of these forces influencing the ith cell is described by the effective force vector $\mathbf{f}^i \in R^D$. The random force $\mathbf{w}^i$ scaled with σ accounts for stochastic nature of sensed extracellular signals and complex mechanical forces influencing cell motility. We model this force as a D dimensional Gaussian white noise process of unit intensity $\mathbf{W} = \mathbf{I}_{D\times D}$, and uncorrelated with measurement errors.

In our model, the relation between the force and velocity is described by the transfer function with the single real pole $-c$, $c \geq 0$. The reason for this lies in the fact that available data presenting the traveled cell distance versus the square root

of time $\sqrt{t}$ are bent for the small values of the time and this is what this simple model predicts (see Fig. 4 and Appendix A).

Only within the limit of large $c \to \infty$ does the curvature of the diagram vanish, which means that even the highest frequency components of the force propagate to the velocity. This results in the Brownian model of cell motility, which seems unrealistic, because it is expected that the mechanical structure of a cell has low-pass frequency characteristics.

In the time domain, our model of the cell i motility is given by the stochastic differential equation with the force term:

$$\dot{\mathbf{x}}^i(t) = \mathbf{v}^i(t) \tag{2}$$

$$\dot{\mathbf{v}}^i(t) = -c\mathbf{v}^i(t) + \sigma\mathbf{w}^i(t) + \mathbf{f}^i(t) \tag{3}$$

We assume that the force $\mathbf{f}^i(t)$ results from a time-stationary force field, which means that the force sensed by the cell depends only on its position. Consequently, we can write $\mathbf{f}^i(t) = \mathbf{F}(\mathbf{x}^i(t))$, where function $\mathbf{F}(\mathbf{x})$ maps the position $\mathbf{x}$ to the force vector and defines the time-stationary force field that we estimate in this work. In the multi-agent literature [12], the right-hand side of (3) is a control of the agent motility, i.e., cell motility. The structure of control and stability analysis has been discussed in [12] and the influence of stochasticity term in [13].

Let us define the column vector $\mathbf{X}^i = [\mathbf{x}^i; \mathbf{v}^i]_{2D\times 1}$, the so-called state vector. Now, we can write the motility and observation model in the matrix form as

$$\dot{\mathbf{X}}^i(t) = \mathbf{A_c}\mathbf{X}^i(t) + \mathbf{L_c}\ \mathbf{w}^i(t) + \mathbf{B_c}\mathbf{f}^i(t) \tag{4}$$

$$\mathbf{y}^i(t) = \mathbf{C_c}\mathbf{X}^i(t) + \theta^i(t)$$

in which matrices $\mathbf{A_c}$, $\mathbf{L_c}$, $\mathbf{C_c}$, as well as the corresponding noise intensity matrix $\mathbf{W}$ can be easily identified (see Appendix

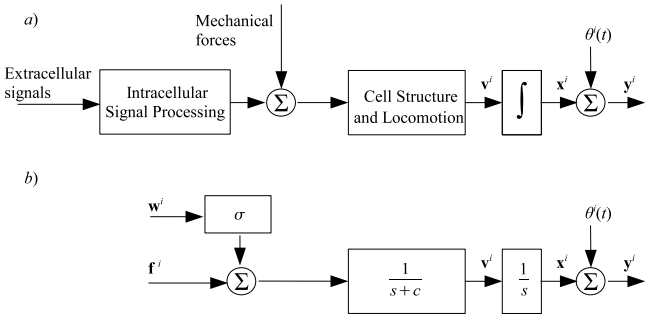

Fig. 3. Time-continuous cell motility model: *a*) General model, *b*) Stochastic motility model

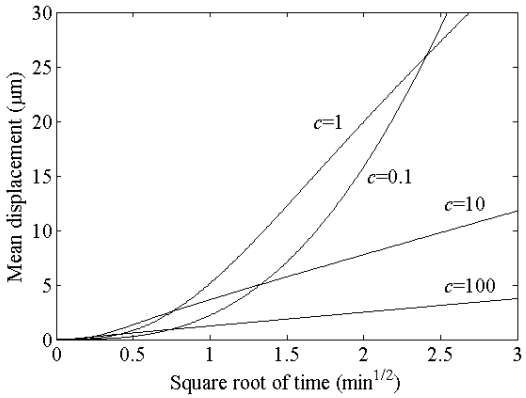

Fig. 4. Cell displacements versus the square root of traveled time, parameters $\sigma = 10$ and $c = 0.1,\ 1,\ 10$ and 100.

B). Since we are dealing with sampled data, it is useful to introduce a discrete time model

$$\begin{aligned} \mathbf{X}^i(k+1) &= \mathbf{A_d}\mathbf{X}^i(k) + \mathbf{L_d}\ \mathbf{w}^i(k) + \mathbf{B_d}\mathbf{f}^i(k) \\ \mathbf{y}^i(k) &= \mathbf{C_d}\mathbf{X}^i(k) + \theta^i(k) \end{aligned} \tag{5}$$

The definitions of the corresponding matrices $\mathbf{A_d}$, $\mathbf{L_d}$ are provided in Appendix B. The variable k corresponds to the time point t_k at which the position vector $\mathbf{y}^i$ is sampled along the ith cell trajectory. We do not provide here the expression for the matrix $\mathbf{B_d}$ because it depends on properties of the continuous signal $\mathbf{f}^i(t)$ [15]. Moreover, in the next section we will incorporate the signal $\mathbf{f}^i(t)$ into the state vector.

The distance and time units that we use from here on are *μm* and *min*. In this paper, we assume that the parameters σ and c of the model are equal for the same cell type. Based on available data, we take these parameters to have values $\sigma = 10$ and $c = 1$. The intensity of the measurement error Θ is a diagonal matrix with diagonal elements equal to 2.5^2, corresponding to approximately one-quarter (1/4) of the expected cell diameter in the case of T- or B-lymphocytes.

4 Force Model and Force Estimation

The force field $\mathbf{F}$ that we estimate is stationary and depends only on the position $\mathbf{x}$. One way to estimate the force field is to assume an analytical shape of the field, parameterize the shape and estimate its parameters. The drawback of this approach is that the assumed form of the field can be unrealistic. In the approach that we are presenting here, we avoid any kind of structural assumptions about the function $\mathbf{F}(\mathbf{x})$, and we exploit the information about the force field from cell trajectory data.

Under assumption that the force field $\mathbf{F}(\mathbf{x})$ is stationary in time, the force as sensed by the ith cell is $\mathbf{f}^i(t) = \mathbf{F}(\mathbf{x}^i(t))$. Our approach to estimate $\mathbf{F}(\mathbf{x})$ is to estimate first the forces influencing cell motility along each individual cell trajectory, then use these estimations to integrate a map that visualizes the force field, which is explained in Section 7.

Our knowledge about the force $\mathbf{f}^i(t)$ is minimal and trajectory dependent. If the field is smooth and the cell motility is a stochastic process, the signal $\mathbf{f}^i(t)$ will be stochastic, too. In the other limit, if the stochastic motility component is of small

intensity, then $\mathbf{f}^i(t)$ will be smooth and possibly well described by a polynomial approximation. To include both possible limits, we model $\mathbf{f}^i(t)$ as the random process

$$\dot{\mathbf{f}}^i(t) = \sigma_F \mathbf{w}_\mathbf{F}^i(t) \tag{6}$$

The parameter σ_F scales the intensity of Gaussian white noise vector $\mathbf{w}_\mathbf{F}^i(t)$, which has the dimension D and is uncorrelated with either $\mathbf{w}^i(t)$ or $\theta^i(t)$. Samples from this stochastic model, although with a small probability of realization, also correspond to the variety of deterministic functions, including those with smooth force variations. The intensity of the expected variations of the force is included using the parameter σ_F. The force with faster expected variations is modeled using a larger σ_F. The force model (6) can be included into the model (5) and it results in the difference equation

$$\begin{aligned} \tilde{\mathbf{X}}^i(k+1) &= \mathbf{A}\tilde{\mathbf{X}}^i(k) + \mathbf{L}\,\tilde{\mathbf{w}}^i(k) \\ \mathbf{y}^i(k) &= \mathbf{C}\tilde{\mathbf{X}}^i(k) + \tilde{\theta}^i(k) \end{aligned} \tag{7}$$

in which the force $\mathbf{f}^i(k)$ is incorporated into the augmented state vector $\tilde{\mathbf{X}}^i = [\mathbf{X}^i; \mathbf{f}^i]_{3D\times 1}$ of the dimension $3D \times 1$ (see Appendix B).

The optimal Bayesian estimation of the state vector of the difference model, such as (7), is a well-studied problem [14]. In this problem, the samples $k = 1, k = 2, \ldots k = N$ are all available at the time point at which the state estimation is computed. This is the so-called fixed interval smoothing problem.

To avoid accumulation of numerical errors and decrease the amount of matrix inversions, the realization of the used optimal smoother is in the so-called Rauch-Tung-Striebel (RTS) form of the fixed interval optimal smoother [14]:

$$\hat{\mathbf{X}}^i(k) = \hat{\mathbf{X}}_\mathbf{F}^i(k) + \mathbf{K_k}[\hat{\mathbf{X}}^i(k+1) - \hat{\mathbf{X}}_\mathbf{F}^{i-}(k+1)] \tag{8}$$

$$\mathbf{K_k} = \mathbf{P_F}^i(k)\mathbf{A}^T\mathbf{P_F}^{i-}(k+1), \;\; \hat{\mathbf{X}}^i(k) = \hat{\mathbf{X}}_\mathbf{F}^i(k) \tag{9}$$

In our case, the computed state estimations $\hat{\mathbf{X}}^i(k) = [\hat{\mathbf{x}}^i(k); \hat{\mathbf{v}}^i(k); \hat{\mathbf{f}}^i(k)]$ include the estimation of positions $\hat{\mathbf{x}}^i(k)$, velocities $\hat{\mathbf{v}}^i(k)$ and forces $\hat{\mathbf{f}}^i(k)$, for all $k = 1, \ldots N$. The covariance matrix of the state vector estimation is

$$\mathbf{P}^i(k) = \mathbf{P_F}^i(k) + \mathbf{K_k}[\mathbf{P}^i(k+1) - \mathbf{P_F}^{i-}(k+1)]\mathbf{K_k^T}, \tag{10}$$

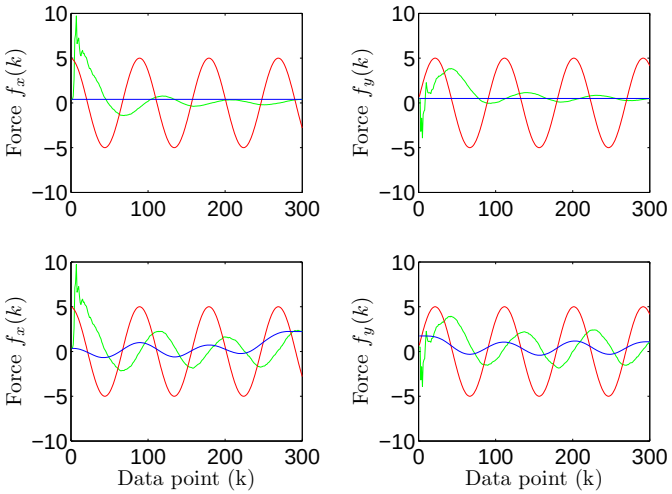

Fig. 5. The force estimation $\sigma_F = 0$ (top) and $\sigma_F = 0.1$ (bottom): true force (red), the forward (Kalman filter) iteration (green), the backward iteration (blue). The true force is defined by expression (11).

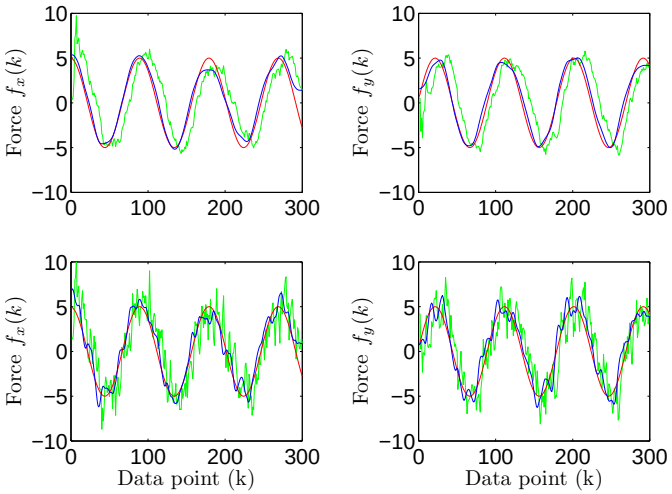

Fig. 6. The force estimation $\sigma_F = 1$ (top) and $\sigma_F = 5$ (bottom): true force (red), the forward (Kalman filter) iteration (green), the backward iteration (blue). The true force is defined by expression (11).

with $\mathbf{P}^i(N) = \mathbf{P_F}^i(N)$. The presented RTS formulation of the smoother includes the forward iteration, which implements the Kalman filter for computing vectors $\hat{\mathbf{X}}_\mathbf{F}$, $\hat{\mathbf{X}}_\mathbf{F}^{i-}$ and matrices $\mathbf{P_F}^i$, $\mathbf{P_F}^{i-}$, as well as the backward iteration presented above. For details on the Kalman filter, see Appendix C.

5 Force estimation along the trajectory

Among all the parameters included in the optimal smoother, the parameter σ_F can be considered as the tuning parameter. The following examples illustrate how this parameter influences the force estimation and that the stochastic model is general enough even in the case when the $\mathbf{f}^i(t)$ is smooth and deterministic.

Here, we generate the cell trajectory based on the model (5), and the force that is

$$\mathbf{f}(k) = \begin{bmatrix} f_x(k) \\ f_y(k) \end{bmatrix} = \begin{bmatrix} 5\cos(4k\pi/180) \\ 5\sin(4k\pi/180) \end{bmatrix} \tag{11}$$

We are dealing here with a single cell and the index i is omitted from the notation. To make it simple, we use here the two-dimensional motility model $D = 2$, with parameters $\sigma = 1$, $c = 1$, $\mathbf{W} = diag\{1,1\}$ and $\mathbf{\Theta} = diag\{2.5^2, 2.5^2\}$.

To apply the smoother, we need to take an initial guess for the state vector estimation $\hat{\mathbf{X}}(0)$; thus, we use

$$\mathbf{x}(0) = \mathbf{y}(0) \text{ and } \mathbf{v}(0) = \frac{1}{\mathrm{t}_1 - \mathrm{t}_0}(\mathbf{y}(1) - \mathbf{y}(0)) \tag{12}$$

because the observed values $\mathbf{y}(0)$ should be close to the true cell position. For the components of $\hat{\mathbf{X}}(0)$, relating to the force $\mathbf{f}(0)$, we use the zero vector. Following the same reasoning, we make use of the following covariance matrix of the initial state:

$$\mathbf{P}(0) = \begin{bmatrix} \mathbf{\Theta}_{2\times 2} & \mathbf{0}_{2\times 2} & \mathbf{0}_{2\times 2} \\ \mathbf{0}_{2\times 2} & \frac{2\mathbf{\Theta}}{t_1 - t_0} & \mathbf{0}_{2\times 2} \\ \mathbf{0}_{2\times 2} & \mathbf{0}_{2\times 2} & 10^2\mathbf{I}_{2\times 2} \end{bmatrix} \tag{13}$$

In the initial state guess $\hat{\mathbf{X}}(0)$, the only arbitrary value is the zero force vector. Therefore, in the covariance vector $\mathbf{P}(0)$, we assume that the standard deviation of the force is large and we take value 10.

First, we consider the case when $\sigma_F = 0$. The result of the smoothing algorithm is presented in the top panels of Fig.5. We can see that, in the forward iteration, the force estimation changes with more data points included. When the last data point is included, the estimated force is the best estimate based on the assumption $\sigma_F = 0$. Therefore, it is obvious why, in this case, the backward iteration does not improve the force estimation. The smoother estimate of the force, for all k, is identical to the last estimate of the Kalman filter in the forward iteration, which is the well-known result of the estimation theory [14].

In the bottom panels of Fig. 5, we show the result when the parameter σ_F is slightly increased. Now $\sigma_F = 0.1$, and we can see that the estimations of the forward and backward smoother iterations are different. In this case, the improvement gained by the backward iteration is considerable if we compare the phase shift between the estimated force and the true force time signal.

By increasing the parameter $\sigma_F = 1$, we get a better match between the true force and the estimation in the phase and amplitude (see Fig. 6, top). In this case, σ_F is large enough, so that the smoother can follow the speed of the force variations.

By increasing σ_F, the smoother is able to follow even faster force variations. However, not only does a larger value for σ_F extend the dynamical range for the forces that the smoother can estimate, but it also results in a smaller attenuation of the noise propagation to the force estimation. This is illustrated in the bottom panels of Fig. 6, resulting from the smoother with $\sigma_F = 5$. We can notice that the force estimation still matches the amplitude and phase of the true signal, but the estimation is noisy.

These four numerical examples primarily illustrate that the force estimation along the trajectory and based on stochastic force models is feasible. They also show that the value of parameter σ_F should be small enough to suppress the propagation of the noise to the estimated force, but still large enough to follow the force variation. When the parameter value is large enough, it influences the noise of estimates and not their expected values. Therefore, we see this parameter as a smoothing parameter of the force field visualization method that will be explained in Section 7.

6 Uniform field estimation

The relation between estimation performance and the cell motility model parameters, dimensions of the visual field, as well as the direction and intensity of the force which is to be estimated, is not simple. For example, one can expect that the strong force is easier to identify and with more confidence due to the larger cell displacement. On the other hand, the force field with a strong average value removes cells faster from the visual field and this ultimately results in a fewer data points that are processed by the estimator. Fewer data points usually result in a higher uncertainty of the force estimation. Here we propose a method for the uniform force field estimation based on an insight into the relation of the estimation uncertainty and trajectory lengths.

Here, we deal with the uniform force field, i.e., $\mathbf{F}(\mathbf{x}) = \mathbf{F}$ and $\mathbf{f}^i(t) = \mathbf{F}$ for any cell i, and the model (5) with parameters $c = 1$, $\sigma = 10$, $\mathbf{W} = diag\{1,1,1\}$, $\mathbf{\Theta} = diag\{2.5^2, 2.5^2, 2.5^2\}$ that are identified from *in vivo* experimental data. The diagram in Fig. 7 shows the square root of the diagonal terms $[\mathbf{S}]_{11} = [\mathbf{S}]_{22} = [\mathbf{S}]_{33}$ of matrix $\mathbf{S}$, which is the submatrix of the Kalman filter covariance matrix $\mathbf{P}$ corresponding only to the force components, i.e.,

$$[\mathbf{S}]_{ij} = [\mathbf{P}]_{2D+i,2D+j}, \quad i,j = 1,2,3 \; D = 3 \tag{14}$$

All these matrices can be computed based on the model parameters and $\sigma_F = 0$. The diagonal terms $[\mathbf{S}]_{ii}$, $i = 1,2,3$ are equal due to the symmetry of our model regarding the change of coordinates.

Based on Fig.7, we can see that the optimal smoother with parameter $\sigma_F = 0$ (constant force assumption) cannot shrink the standard deviation of the force estimation below 10% of initial uncertainity for less than 100 samples of the trajectory. On the other hand, the cell trajectory length from experiments rarely goes over 100 samples. The typical number of samples is between 15 and 35. For this reason, and in order to increase the precision of the force estimation, it is beneficial to rely on the data across observed cell trajectories.

In the case of a constant force, estimations obtained for different trajectories can be integrated based on the maximum

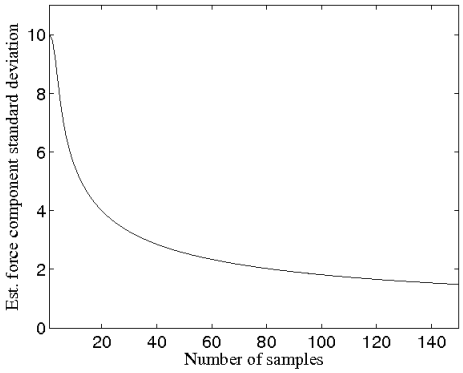

Fig. 7. The standard deviation of the constant force estimation component; the fixed interval smoother parameter $\sigma_F = 0$

likelihood approach. Let us assume that we have applied the optimal force estimator with $\sigma_F = 0$ to obtain the sequence of force estimations $\hat{\mathbf{F}}^i$, $i = 1,2,\ldots$ and their covariance matrices $\mathbf{S}^i$. Under the assumption of the linear model (5) and the Kalman filter theory [14], the distribution of the estimated force is Gaussian, so that the joint likelihood of the estimated values is (see Appendix D)

$$\mathcal{L} = \prod_{i=1,2,\ldots} \mathcal{N}(\hat{\mathbf{F}}^i - \overline{\mathbf{F}}, \mathbf{S}^i) \tag{15}$$

where $\mathcal{N}(\cdot, \mathbf{S}^i)$ is a Gaussian distribution with zero vector mean value and covariance matrix $\mathbf{S}^i$. The vector $\overline{\mathbf{F}}$ denotes the expected value of the constant force based on data from all cell trajectories. This expected value can be found by minimizing the log of likelihood $\mathcal{L}$, which results in the weighted average

$$\overline{\mathbf{F}} = \left[\sum_{i=1,2,\ldots} [\mathbf{S}^i]^{-1} \right]^{-1} \left[\sum_{i=1,2,\ldots} [\mathbf{S}^i]^{-1} \hat{\mathbf{F}}^i \right] \tag{16}$$

We can use the optimal force estimator with $\sigma_F = 0$ and the above expression when we expect a uniform force field inside the visual field. However, we use the same expression for the estimation of a non-uniform force field. We will discuss this in the following section.

7 Non-uniform field estimation

For the estimation of the force field $\mathbf{F}(\mathbf{x})$ that influences cell motility, we propose a two-step strategy: first, to estimate forces $\mathbf{f}^i(k)$ that influence the cell motility at each observed cell position; second, to integrate all estimated values into a map that represents the force field, taking into account that the field $\mathbf{F}(\mathbf{x})$ is stationary in time.

From the results of the previous sections, we can see that we should assume the intensity of the variation of the forces $\mathbf{f}^i(k)$ and, then, properly tune the smoothing parameter σ_F. To improve the consistency of our estimation, instead of starting

from $\mathbf{f}^i(k)$ as zero vectors, we estimate first the force $\overline{\mathbf{F}}$ in the same way that we estimate the constant force in the previous section. Then, we use this vector as an initial guess $\hat{\mathbf{f}}^i(0)$ for the estimation of the force along ith cell trajectory at the kth time point, $\hat{\mathbf{f}}^i(k)$. The motivation for this comes from the fact that the force $\overline{\mathbf{F}}$ is the best constant force that can describe all cell trajectories; thus, it is sensible to use it as an initial guess for $\hat{\mathbf{f}}^i(0)$ and all $i = 1,2\ldots$. With this guess and the smoothing algorithm, we can compute the estimates of the forces $\hat{\mathbf{f}}^i(k)$ at the cell positions $\hat{\mathbf{x}}^i(k)$ that we use in the second step.

Each estimate $\hat{\mathbf{f}}^i(k)$ corresponds to the cell position $\hat{\mathbf{x}}^i(k)$; in other words, we make identification that the force field estimation $\hat{\mathbf{F}}(\hat{\mathbf{x}}^i(k)) = \hat{\mathbf{f}}^i(k)$. However, to build a consistent estimation of the force field, we also assume that each cell is influenced by the same force at the same position in the space. Taking this into account, we can say that for $\hat{\mathbf{x}}^j(k_m) \approx \hat{\mathbf{x}}^i(k_n)$ and, obviously, $k_m \neq k_n$, we have $\hat{\mathbf{F}}(\hat{\mathbf{x}}^j(k_m)) \approx \hat{\mathbf{F}}(\hat{\mathbf{x}}^i(k_n))$.

To estimate the field, we divide our visual field into R rectangular regions. We denote each of these regions as Ω_r, with $r = 1,2,\ldots R$ being the unique index of the region. Moreover, we define the set $\mathbf{In}(\Omega_r)$ as

$$\mathbf{In}(\Omega_r) = \{(i,k)|\hat{\mathbf{x}}^i(k) \in \Omega_r\} \tag{17}$$

Then, the force field $\mathbf{F}(\mathbf{x})$ for each region r, i.e., for $x \in \Omega_r$, can be estimated as the weighted average

$$\hat{\mathbf{F}}(\mathbf{x} \in \Omega_r) = \left[\sum_{(i,k)\in\mathbf{In}(\Omega_r)} [\mathbf{S}^i(k)]^{-1}\right]^{-1} \left[\sum_{(i,k)\in\mathbf{In}(\Omega_r)} [\mathbf{S}^i(k)]^{-1}\hat{\mathbf{f}}^i(k)\right] \tag{18}$$

This expression is identical to (16), except for the summation and product that go over all the couples (i,k) from the set $\mathbf{In}(\Omega_r)$ of the specific region Ω_r (see Appendix D).

We apply the described approach for the estimation of the force field to 40 cell trajectories generated from the model (5), $\sigma = 10$, $c = 1$, $\mathbf{W} = diag\{1,1,1\}$, $\mathbf{\Theta} = diag\{2.5^2, 2.5^2, 2.5^2\}$, with the same geometrical constraints as in the previous section. In the example, we devide the visual field into $R = 100$ rectangular regions of $20 \times 15\mu m$ and generate the data assuming the force field

$$\mathbf{F}(\mathbf{x}) = \begin{bmatrix} 5 \\ 5\sin(\pi x/100) \\ 0 \end{bmatrix} \tag{19}$$

To include the fact that experimental data usually neglect short cell trajectories, we generated 200 cell trajectories and, then, randomly chose 40 cell trajectories, which had more than 16 points. Samples of the generated tracks are depicted in Fig. 2 in such a way that the first point of each trajectory is translated to the origin (0,0).

The result of our approach to force field estimation is presented in Fig. 8. The red arrows represent the force $\overline{\mathbf{F}}$ used as the initial condition for the estimation of $\mathbf{f}^i(k)$. To compute the field estimate $\hat{\mathbf{F}}$, we use a decreasing sequence of parameter σ_F, starting from considerable large $\sigma_F = 10$, to obtain a series of estimations. When the region Ω_r contains less than three trajectory points, we skip averaging the forces estimated in the region assuming that we have little data for averaging. For all regions Ω_r with more than three trajectory points, we compute the average $\hat{\mathbf{F}}$ and depict it with a blue thick arrow. The largest value of σ_F for which the estimations are consistent across the data generated from different simulation runs is $\sigma_F = 0.1$. The blue arrows visualize the estimated force field from one of the simulation generated data sets.

The quality of the field estimation depends on cell trajectories; generally, the more recorded trajectories in the square region Ω_r, the more estimates per region available for averaging. In our case, the force component along the x axis is constant 5 (see equation (19)). The y component changes from 0 at points with $x = 0$ to 5 at points $x = 50$ and, then, back to 0 at points $x = 100$. Then, this force component changes its sign and becomes negative -5 at points with $x = 150$, and again 0 at $x = 200$. The force estimations that we acquired in Fig. 8 follow the above-described changes and give an insight into the field shape, although without great precision. The constant force $\overline{\mathbf{F}}$ (red arrows), which estimates the average component of forces in the visual field, is reliably estimated.

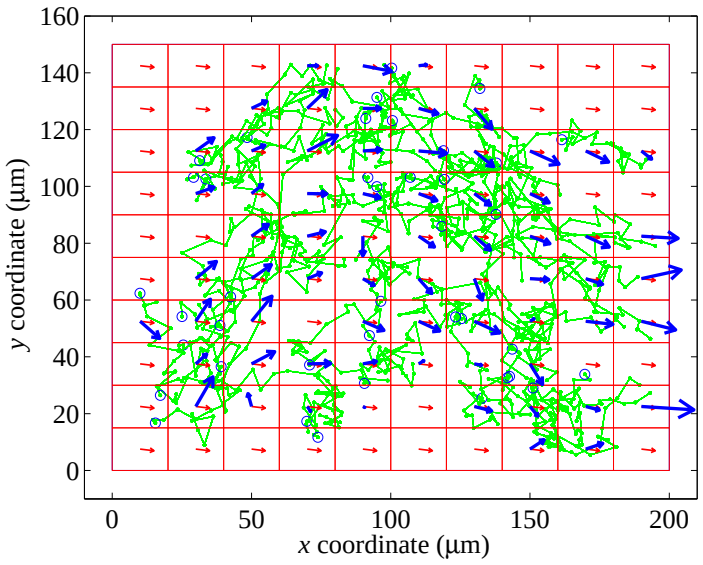

Fig. 8. Result of the force field estimation: the cell trajectories (green); the constant force $\overline{\mathbf{F}}$ (red arrows), the smoother estimation $\hat{\mathbf{F}}$ (blue thick arrows); the interval smoother parameter $\sigma_F = 0.1$. The true field is defined by expression (19).

8 Conclusions

Following technological breakthrough in imaging, we are now able to observe the evolution of *in vivo* immune system interactions. In this work, we have developed an approach for the estimation of the force field influencing cell motility. For this approach, we used the optimal smoother estimator of the forces and formed a map that visualizes the force field

based on its estimations. We did not impose any analytical constraints on the force field. We introduced a spatial correlation between the forces by integrating estimations over a grid of rectangular regions. Consequently, the force field is estimated and visualized by the average forces assigned to each rectangular region.

Using the proposed method, we are confident to estimate the intensity and direction of the major constant component of the force field. We also find that the directions of the force field are satisfactorily identified. In order to apply the method for the analysis of imaging data routinely, the rapid adjustment of the estimator parameters is important. For this reason, we need further consideration of real data, including data collected from different immune system interactions and different organs.

Estimation of the forces that influence motility of immune system cells provides an additional powerful tool for the analysis of two-photon microscopic data. Our results show that real-time video images are a source of data enabling us visualization, which can be used for studying intriguing spatio-temporal phenomena inside immune system organs. We hope that our and similar approaches can fill the existing gap between contemporary technology and quantitative data analyses present in the field.

Appendix A

For the illustration, we will derive the cell displacement for the case $D = 2$. In the absence of the force $\mathbf{f}^i = 0$, we can derive that the covariance of the x and y components of the position is

$$\Sigma_{xx}(t) = \Sigma_{yy}(t) = \Sigma(t) = 2\sigma^2 \left(\frac{t}{2c^2} - \frac{3}{4c^3} + \frac{1}{c^3} e^{-ct} - \frac{1}{4c^3} e^{-2ct} \right) \tag{20}$$

The probability density function of the position (x,y) is Gaussian with the covariance $\Sigma(t)$ and by introducing the radial displacement $\delta = \sqrt{x^2+y^2}$ we find that the probability density function of the displacement δ and the corresponding mean value are

$$p(\delta) = \frac{\delta}{\sigma^2} e^{-\frac{\delta^2}{2\Sigma(t)}}, \quad E\{\delta(t)\} = \sqrt{\Sigma(t)\frac{\pi}{2}} \tag{21}$$

The mean value scales with $\sqrt{t}$ for $t \to \infty$.

Appendix B

For the motility model, in two (D=2) or three (D=3) dimensions, the matrices are

$$\mathbf{A_c} = \begin{bmatrix} \mathbf{0}_{D\times D} & \mathbf{I}_{D\times D} \\ \mathbf{0}_{D\times D} & -c\mathbf{I}_{D\times D} \end{bmatrix},\ \mathbf{L_c} = \begin{bmatrix} \mathbf{0}_{D\times D} \\ \sigma\mathbf{I}_{D\times D} \end{bmatrix},\ \mathbf{B_c} = \begin{bmatrix} \mathbf{0}_{D\times D} \\ \mathbf{I}_{D\times D} \end{bmatrix},\ \mathbf{C_c} = \begin{bmatrix} \mathbf{I}_{D\times D}\ \mathbf{0}_{D\times D} \end{bmatrix} \tag{22}$$

Let us intoduce the transition matrix

$$\mathbf{\Phi}(t_k,t) = e^{\mathbf{A_c}(t_k-t)} \tag{23}$$

Then the state covariance of the continuous model

$$\dot{\mathbf{X}} = \mathbf{A_c}\mathbf{X} + \mathbf{L_c}\mathbf{w}(t) \tag{24}$$

$$\mathbf{Y} = \mathbf{C_c}\mathbf{X} + \theta(t) \tag{25}$$

sampled at regularly sampled time instants t_k, $t_{k+1} - t_k = \Delta$ is [14]

$$\mathbf{P_{k+1}} = \mathbf{\Phi}(t_{k+1},t_k)\mathbf{P}_k\mathbf{\Phi}(t_{k+1},t_k)^T + \int_{t_k}^{t_{k+1}} \mathbf{\Phi}(t_{k+1},t)\mathbf{L_c}\mathbf{W}\mathbf{L_c}^T\mathbf{\Phi}(t_{k+1},t)^T dt \tag{26}$$

Therfore, the regularly sampled continous-time stochastic model (24), with constant matrices $\mathbf{A_c}$, $\mathbf{L_c}$ and $\mathbf{W} = \mathbf{I}$ being the covariance of the vector $\mathbf{w}$, can be represented as the discrete-time stochastic process

$$\mathbf{X}(k+1) = \mathbf{A_d}\mathbf{X}(k) + \mathbf{L_d}\mathbf{w} \tag{27}$$

$$\mathbf{Y}(k) = \mathbf{C_d}\mathbf{X}(k) + \theta(k) \tag{28}$$

where

$$\mathbf{A_d} = e^{\mathbf{A_c}\Delta},\ \mathbf{L_d}\mathbf{L_d}^T = \int_0^{\Delta} e^{\mathbf{A_c}\Delta}\mathbf{L_c}\left(e^{\mathbf{A_c}\Delta}\mathbf{L_c}\right)^T dt,\ \mathbf{C_d} = \mathbf{C_c} \tag{29}$$

To compute samples of the model (31)-(32), the Kalman filter and the smoother, we only need the matrix $\mathbf{L_d}\mathbf{L_d}^T$. Therefore, we do not consider the problem of computing the matrix $\mathbf{L_d}$.

In the case of matrices (25), we have

$$\mathbf{A_d} = \begin{bmatrix} \mathbf{I}_{D\times D} & \frac{1-e^{-c\Delta}}{c}\mathbf{I}_{D\times D} \\ 0 & e^{-c\Delta}\mathbf{I}_{D\times D} \end{bmatrix}, \ \mathbf{L_d}\mathbf{L_d}^T = \sigma^2 \begin{bmatrix} (-\frac{e^{-2c\Delta}}{2c^3} + \frac{2e^{-c\Delta}}{c^3} + \frac{\Delta}{c^2} - \frac{3}{2c^3})\mathbf{I}_{D\times D} & (\frac{e^{-2c\Delta}}{2c^2} - \frac{e^{-c\Delta}}{c^2} + \frac{1}{2c^2})\mathbf{I}_{D\times D} \\ (\frac{e^{-2c\Delta}}{2c^2} - \frac{e^{-c\Delta}}{c^2} + \frac{1}{2c^2})\mathbf{I}_{D\times D} & (-\frac{e^{-2c\Delta}}{2c} + \frac{1}{2c})\mathbf{I}_{D\times D} \end{bmatrix} \tag{30}$$

In the case of the augmented state discrete time model (6), the matrices $\mathbf{A}$ and $\mathbf{L}$ are defined by expression (29) where $\mathbf{A} = \mathbf{A_d}$, $\mathbf{L} = \mathbf{L_d}$, $\mathbf{C} = \begin{bmatrix} \mathbf{C_c} & \mathbf{0}_{D\times D} \end{bmatrix}$ and

$$\mathbf{A_c} = \begin{bmatrix} \mathbf{0}_{D\times D} & \mathbf{I}_{D\times D} & \mathbf{0}_{D\times D} \\ \mathbf{0}_{D\times D} & -c\mathbf{I}_{D\times D} & \mathbf{I}_{D\times D} \\ \mathbf{0}_{D\times D} & \mathbf{0}_{D\times D} & \mathbf{0}_{D\times D} \end{bmatrix}, \ \mathbf{L_c} = \begin{bmatrix} \mathbf{0}_{D\times D} & \mathbf{0}_{D\times D} \\ \sigma\mathbf{I}_{D\times D} & \mathbf{0}_{D\times D} \\ \mathbf{0}_{D\times D} & \sigma_F\mathbf{I}_{D\times D} \end{bmatrix} \tag{31}$$

This results in

$$\mathbf{A} = \begin{bmatrix} \mathbf{I}_{D\times D} & \frac{1-e^{-c\Delta}}{c} & -\frac{1-e^{-c\Delta}}{c^2} + \frac{\Delta}{c} \\ 0 & e^{-c\Delta} & \frac{1-e^{-c\Delta}}{c} \\ 0 & 0 & 1 \end{bmatrix} \text{ and } \mathbf{L}\mathbf{L}^T = \begin{bmatrix} \Lambda_{11}\mathbf{I}_{D\times D} & \Lambda_{12}\mathbf{I}_{D\times D} & \Lambda_{13}\mathbf{I}_{D\times D} \\ \Lambda_{12}\mathbf{I}_{D\times D} & \Lambda_{22}\mathbf{I}_{D\times D} & \Lambda_{23}\mathbf{I}_{D\times D} \\ \Lambda_{13}\mathbf{I}_{D\times D} & \Lambda_{23}\mathbf{I}_{D\times D} & \Lambda_{33}\mathbf{I}_{D\times D} \end{bmatrix} \tag{32}$$

where

$$\Lambda_{11} = \sigma_F^2\left(\frac{e^{-2c\Delta}}{2c^4} - \frac{e^{-c\Delta}}{c^4} + \frac{\Delta e^{-c\Delta}}{c^3} + \frac{\Delta^2}{2c^2} - \frac{\Delta}{c^3}\right) + \sigma^2\left(-\frac{e^{-2c\Delta}}{2c^3} + \frac{2e^{-c\Delta}}{c^3} + \frac{\Delta}{c^2}\right) \tag{33}$$

$$\Lambda_{12} = \sigma_F^2\left(\frac{2e^{-2c\Delta}}{c^4} - \frac{e^{-c\Delta}}{c^4} + \frac{\Delta e^{-c\Delta}}{c^3} + \frac{\Delta^2}{2c^2} - \frac{\Delta}{c^3} + \frac{3}{c^4}\right) + \sigma^2\left(\frac{1-e^{-c\Delta}}{c^2} - \frac{1-e^{-2c\Delta}}{2c^2}\right) \tag{34}$$

$$\Lambda_{13} = \sigma_F^2\left(\frac{1-e^{-c\Delta}}{c^3} + \frac{\Delta^2}{2c} - \frac{\Delta}{c^2}\right), \ \Lambda_{23} = \sigma_F^2\left(-\frac{1-e^{-c\Delta}}{c^2} + \frac{\Delta}{c}\right) \tag{35}$$

$$\Lambda_{22} = \sigma_F^2 \left(-\frac{e^{-2c\Delta}}{2c^3} + 2\frac{e^{-c\Delta}}{c^3} + \frac{\Delta}{c^2} - \frac{3}{2c^3} \right) + \sigma^2 \frac{1 - e^{-2c\Delta}}{2c},\ \Lambda_{33} = \sigma_F^2 \Delta \tag{36}$$

Appendix C

The Kalman filter iteration is described by the following equations [14]:

$$\hat{\mathbf{X}}_{\mathbf{F}}^{i-}(k+1) = \mathbf{A}\hat{\mathbf{X}}_{\mathbf{F}}^{i}(k) \tag{37}$$

$$\mathbf{P_F}^{i-}(k+1) = \mathbf{A}\mathbf{P_F}^{i}(k)\mathbf{A}^T + \mathbf{L}^T\mathbf{L} \tag{38}$$

$$\hat{\mathbf{X}}^{i}(k) = \hat{\mathbf{X}}_{\mathbf{F}}^{i-}(k) + \mathbf{K_{KF}}[\mathbf{y}^{i}(k) - \mathbf{C}\hat{\mathbf{X}}_{\mathbf{F}}^{i-}(k)] \tag{39}$$

$$\mathbf{P_F}^{i}(k) = [\mathbf{I} - \mathbf{K_{KF}}\mathbf{C}]\mathbf{P_F}^{i-}(k) \tag{40}$$

$$\mathbf{K_{KF}} = \mathbf{P_F}^{i-}(k)\mathbf{C}^T[\mathbf{C}\mathbf{P_F}^{i-}(k)\mathbf{C}^T + \mathbf{\Theta}]^{-1} \tag{41}$$

The first equation (37) is usually referred as the prediction step because it computes the model base prediction for the following time point. Similarly, equation (38) is the model based prediction for the covariance matrices. Both of these values are computed starting from the initial values $\hat{\mathbf{X}}_{\mathbf{F}}^{i}(0)$ and $\mathbf{P_F}^{i}(0)$. Equation (39) is the so-called update step, because it computes the optimal estimation $\hat{\mathbf{X}}^{i}(k)$ based on the prediction $\hat{\mathbf{X}}^{i-}(k)$ and observed data $\mathbf{y}^{i}(k)$. The Kalman filter gain $\mathbf{K_{KF}}$ depends on the prediction covariance matrix $\mathbf{P_F}^{i-}(k)$, which is the covariance matrix of the estimated state vector $\hat{\mathbf{X}}_{\mathbf{F}}^{i-}(k)$.

Appendix D

In the case of the uniform field estimation, the estimations $\hat{\mathbf{F}}^{i}$ and $\hat{\mathbf{F}}^{j}$, $i \neq j$ resulting from trajectories of two different cells can be considered as two independent estimates of the force $\mathbf{F}$. Because of that, their joint probability density function is a product of their individual probability density functions, which are Gaussian according to the theory [14]. Thus, we can say that the likelihood of estimations from all available cell trajectories is

$$\mathcal{L} = \prod_{i=1,2,\ldots} \mathcal{N}(\hat{\mathbf{F}}^{i} - \overline{\mathbf{F}}, \mathbf{S}^{i}) \tag{42}$$

where $\overline{\mathbf{F}}$ is the force $\mathbf{F}$ expected value. Maximization of this likelihood in order to find the estimation $\overline{\mathbf{F}}$ is equivalent to minimization of its negative likelihood

$$-\log \mathcal{L} = \frac{1}{2} \sum_{i=1,2,\ldots} (\hat{\mathbf{F}}^{i} - \overline{\mathbf{F}})^T [\mathbf{S}^{i}]^{-1} (\hat{\mathbf{F}}^{i} - \overline{\mathbf{F}}) + C \tag{43}$$

where C includes all terms independent on $\overline{\mathbf{F}}$. Derivatives of this expression regarding $\overline{\mathbf{F}}$ are equal to zero at the minimum, i.e., $\sum_{i=1,2,...}[\mathbf{S}^i]^{-1}(\hat{\mathbf{F}}^i - \overline{\mathbf{F}}) = \mathbf{0}$ and from this we can conclude that

$$\overline{\mathbf{F}} = \left[\sum_{i=1,2,...}[\mathbf{S}^i]^{-1}\right]^{-1}\left[\sum_{i=1,2,...}[\mathbf{S}^i]^{-1}\hat{\mathbf{F}}^i\right] \tag{44}$$

In the case of the time stationary non-uniform field $\mathbf{F}(\mathbf{x})$, the force estimations along the two different trajectories $\hat{\mathbf{f}}^i(k_n)$ and $\hat{\mathbf{f}}^j(k_m)$, $i \neq j$ are independent random Gaussian vectors. Assuming that $\mathbf{F}(\mathbf{x})$ is constant over the square region Ω_r and neglecting the correlation among estimates from the same cell trajectory, i.e., between $\hat{\mathbf{f}}^i(k_m)$ and $\hat{\mathbf{f}}^i(k_n)$, $k_m \neq k_n$, we can write the likelihood of the force inside the region $\mathbf{F}(\mathbf{x} \in \Omega_r)$ as

$$\mathcal{L} = \prod_{(i,k)\in \mathbf{In}_{\Omega_r}} \mathcal{N}(\hat{\mathbf{f}}^i(k) - \hat{\mathbf{F}}(\mathbf{x} \in \Omega_r)) \tag{45}$$

where $\hat{\mathbf{F}}(\mathbf{x} \in \Omega)$ is the expected value of the force in square region Ω_r, and $\mathbf{In}_{\Omega_r}$ is defined by (17). Using this likelihood and applying steps (42)-(44), we can derive (18).

References

[1] M. J. Miller, S. H. Wei, I. Parker and M.D. Cahalan, *Two-photon imaging of lymphocyte motility and antigen response in intact lymph node*, Science, vol. 296, pp. 1869-1873, 2002.

[2] T. R. Mempel, S. E. Henrickson and U. H. von Andrian, *T-cell priming by dendritic cells in lymph nodes occurs in three distinct phases*, Nature, vol. 427, pp. 154-159, 2004.

[3] C. Sumen, T.R Mempel, I.B. Mazo and U.H. von Andrian, *Intravital Microscopy: Visualizing Immunity in Context*, Immunity, vol. 21, pp. 315-329, 2004.

[4] D. Milutinović and P. Lima, *Cells and Robots: Modeling and Control of Large-Size Agent Populations*, Springer 2007

[5] M.W.M.G. Dissanayake, P. Newman, S. Clark, H.F. Durrant-Whyte and M. Csorba, *A solution to the simultaneous localization and map building (SLAM) problem*, IEEE Transactions on Robotics and Automation, vol. 17, no.3, pp.229-241, 2001.

[6] S. Thrun, W. Burgard and D. Fox, *Probabilistic robotics*, Intelligent robotics and autonomous agents, MIT Press, 2005.

[7] H. R. Bourne and O. Weiner, *A chemical compass*, Nature, vol. 419, pp. 21, 2002.

[8] F. I. Comer and C. A. Parent, *PI 3-Kinases and PTEN: How opposites chemoattract*, Cell, vol. 109, pp. 541-544, 2002.

[9] M. Onsum and C. V. Rao, *A mathematical model for neutrophil gradient sensing and polarization*, PLOS Computational Biology, vol. 3 , pp. 436-459, 2007.

[10] N. Leonard and E. Fiorelli, *Virtual Leaders, Artificial Potentials and coordinated control of groups*, Proceedings of

IEEE International Conference on Decision and Control, pages 2968-2973, 2001.

[11] H. G. Tanner, A. Jadbabaie and G. J. Pappas, *Flocking in Fixed and Switching Networks*, IEEE Transactions on Automatic Control, 52(5):863-868, May 2007.

[12] R. Olfati-Saber, *Flocking for Multi-agent Dynamic Systems: Algorithms and Theory*, IEEE Transactions on Automatic Control, 51(3):401-420, Mar. 2006

[13] M. Kumar, D. Milutinovic and D. Garg, *Role of Stochasticity in Self-Organization of Robotic Swarms*, Proceedings of American Control Conference 2008, Seattle, Washington, USA

[14] A. Gelb, *Applied Optimal Estimation*, M.I.T. press, 1974.

[15] K. J.Astrom, B. Wittenmark, *Computer-controlled Systems : theory and design*, Prentice Hall, 1990.

LIST OF CAPTIONS

Fig. 1. Computer-generated image of a cellular interaction inside the lymph node: T-cells (red) scan dendritic cells (green) [4]

Fig. 2. Two dimensional projection of 40 cell tracks from the 200x150x50 μm visual field provided by two-photon video microscopy (model generated). Each track is translated so that the track begins at the diagram origin. The cells can move in all directions, therefore, the limits for plotting translated trajectories are $\pm 200\mu m$ and $\pm 150\mu m$ along x and y axis, respectively.

Fig. 3. Time-continuous cell motility model: *a*) General model, *b*) Stochastic motility model

Fig. 4. Cell displacements versus the square root of traveled time, parameters $\sigma = 10$ and $c = 0.1,\ 1,\ 10$ and 100.

Fig. 5. The force estimation $\sigma_F = 0$ (top) and $\sigma_F = 0.1$ (bottom): true force (red), the forward (Kalman filter) iteration (green), the backward iteration (blue). The true force is defined by expression (11).

Fig. 6. The force estimation $\sigma_F = 1$ (top) and $\sigma_F = 5$ (bottom): true force (red), the forward (Kalman filter) iteration (green), the backward iteration (blue). The true force is defined by expression (11).

Fig. 7. The standard deviation of the constant force estimation component; the fixed interval smoother parameter $\sigma_F = 0$

Fig. 8. Result of the force field estimation: the cell trajectories (green); the constant force $\overline{\mathbf{F}}$ (red arrows), the smoother estimation $\hat{\mathbf{F}}$ (blue thick arrows); the interval smoother parameter $\sigma_F = 0.1$. The true field is defined by expression (19).

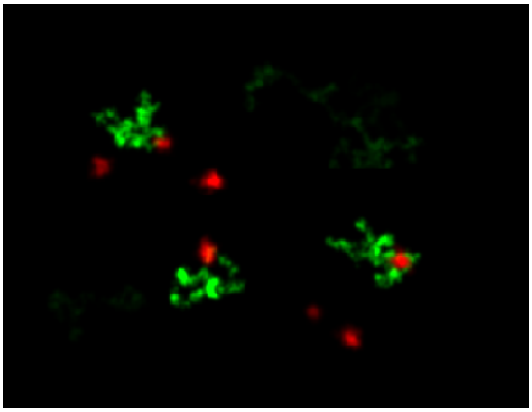

Fig1.eps

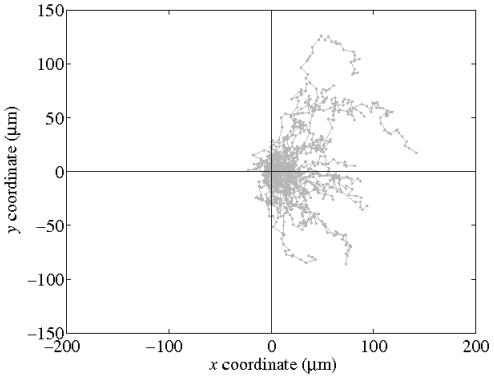
150
100
50
0
−50
−100
−150
−200
−100
0
100
200
y coordinate (μm)
x coordinate (μm)

Fig2.eps

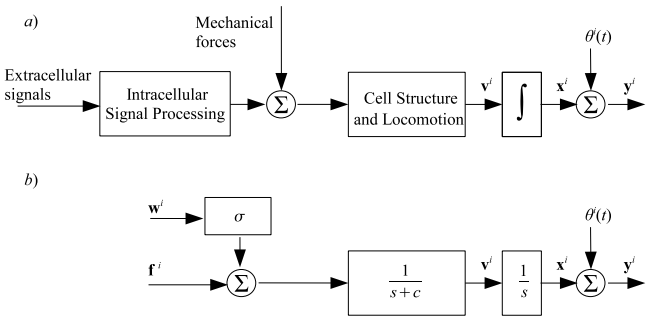
a)
Mechanical forces
Extracellular signals
Intracellular Signal Processing
Cell Structure and Locomotion
b)
σ
1/(s+c)
1/s

Fig3.eps

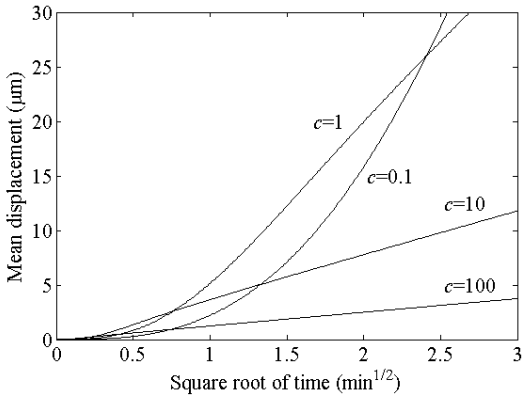
Mean displacement (μm)
Square root of time (min^1/2)
c=1
c=0.1
c=10
c=100
0
5
10
15
20
25
30
0
0.5
1
1.5
2
2.5
3

Fig4.eps

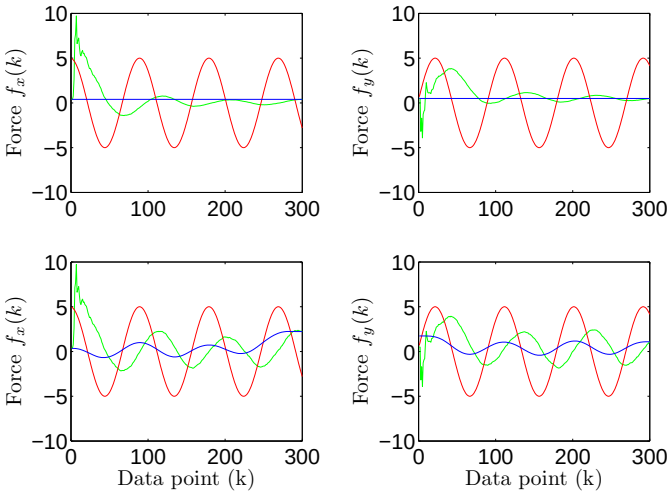
Force $f_x(k)$
Force $f_y(k)$
Force $f_x(k)$
Force $f_y(k)$
Data point (k)
Data point (k)
10
5
0
−5
−10
0
100
200
300

Fig5.eps

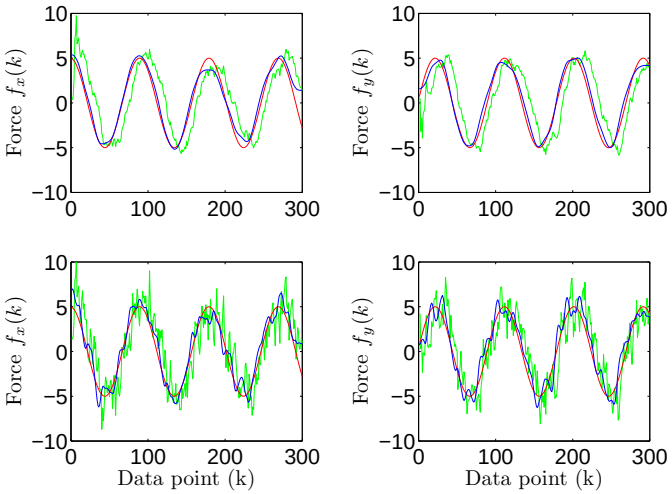
Force $f_x(k)$
Force $f_y(k)$
Force $f_x(k)$
Force $f_y(k)$
Data point (k)
Data point (k)

Fig6.eps

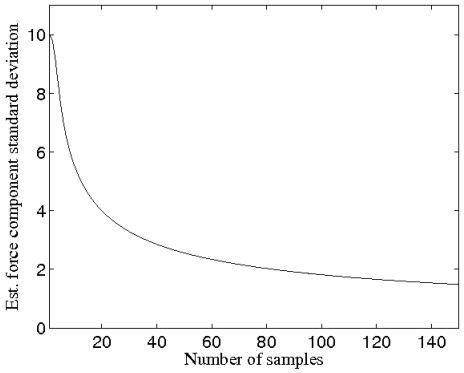
Est. force component standard deviation
Number of samples
0
2
4
6
8
10
20
40
60
80
100
120
140

Fig7.eps

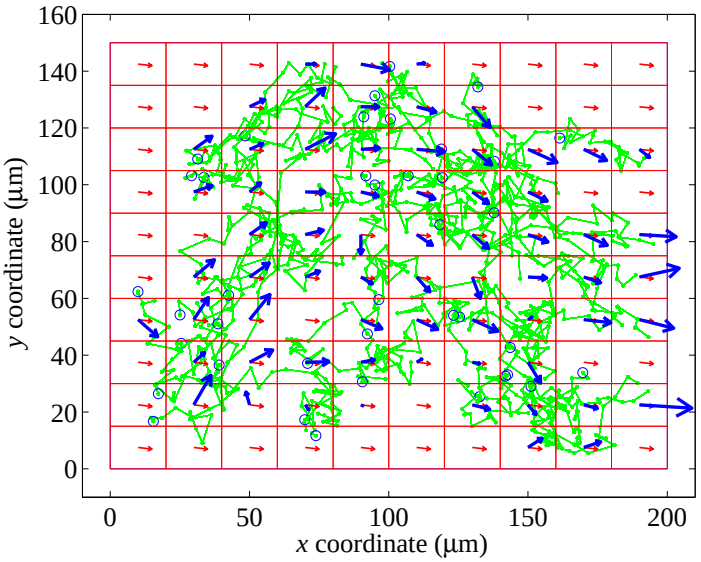
160
140
120
100
80
60
40
20
0
y coordinate (μm)
0
50
100
150
200
x coordinate (μm)

Fig8.eps